Proc. Natl. Acad. Sci. USA
Vol. 92, pp. 10969–10976, November 1995
Biochemistry

This contribution is part of the special series of Inaugural Articles by members of the National Academy of Sciences elected on April 25, 1995.

Lyophilization-induced reversible changes in the secondary structure of proteins

(Fourier-transform infrared spectroscopy/dehydration/α-helix/β-sheet/solid state)

KAI GRIEBENOW AND ALEXANDER M. KLIBANOV*

Department of Chemistry, Massachusetts Institute of Technology, Cambridge, MA 02139

Contributed by Alexander M. Klibanov, August 28, 1995

ABSTRACT **Changes in the secondary structure of some dozen different proteins upon lyophilization of their aqueous solutions have been investigated by means of Fourier-transform infrared spectroscopy in the amide III band region. Dehydration markedly (but reversibly) alters the secondary structure of all the proteins studied, as revealed by both the quantitative analysis of the second derivative spectra and the Gaussian curve fitting of the original infrared spectra. Lyophilization substantially increases the β-sheet content and lowers the α-helix content of all proteins. In all but one case, proteins become more ordered upon lyophilization.**

Consider the common laboratory and bioindustrial process of lyophilization or freeze-drying of aqueous solutions of proteins. Suppose that this lyophilization is carried out such that no irreversible damage to the protein ensues—i.e., when the lyophilized protein is redissolved in water, it exhibits the same properties as prior to lyophilization. The question still remains whether the protein structure in the lyophilized form is native or whether the lyophilization has resulted in reversible protein denaturation. Apart from its biochemical interest, the answer has important biotechnological implications. For example, proteins that have been lyophilized (which is how research and pharmaceutical protein preparations are usually stored) undergo moisture-triggered aggregation (1). To understand the mechanism of this undesirable phenomenon and to develop rational strategies for its prevention, structural information on proteins in the solid—e.g., lyophilized—form is needed. In addition, lyophilized enzymes suspended in organic solvents have proven to be useful synthetic catalysts (2); enzyme structural data should help maximize their performance.

The issue of protein conformation in the lyophilized form is controversial. For example, the results of Fourier-transform infrared (FTIR) spectroscopic investigations of hen egg-white lysozyme were interpreted to indicate that lysozyme structure in either aqueous solution or the lyophilized state is the same (3–6). This conclusion was supported by some hydrogen isotope-exchange studies (6, 7) but contradicted by others (8). Raman (9–11) and solid-state NMR (12) studies have suggested significant (reversible) structural changes occurring in lysozyme upon lyophilization. Likewise, recent hydrogen isotope-exchange/high-resolution NMR (13) and FTIR (14, 15) investigations of various proteins strongly point to lyophilization-induced reversible denaturation.

Recent advances, both instrumentational and conceptual, in FTIR spectroscopy make it a method of choice for examining the structure of solid proteins. This has been illustrated by the scholarly work of Prestrelski *et al.* (14, 15), who have employed this methodology to quantify changes in the secondary structure of proteins caused by lyophilization. Using the second derivatives of the vibrational spectra of proteins in the amide I band region (1600–1720 cm^{-1}), these authors have calculated so-called correlation coefficients which reflect the overall changes in the secondary structure upon lyophilization. This approach, however, yields no quantitative information about changes in the individual structural elements—e.g., percentages of α-helices and β-sheets. This is because although the FTIR bands in the amide I region directly correspond to these secondary structural elements (16, 17), the line broadening in the spectra of lyophilized proteins, combined with strongly overlapping bands, make such quantitation in this region arduous (15, 18). Another spectral region, the amide III band (1220–1330 cm^{-1}), also reflects the secondary structure of proteins (19–21) and has been used to characterize structural changes qualitatively (22–26) and, in aqueous solution, even to quantify the individual secondary structure composition of proteins (19–21, 27).

We have employed the IR amide III band region to investigate quantitatively the reversible changes in the secondary structure of some dozen different proteins occurring upon lyophilization. Consequently, alterations in the individual structural elements have been determined. For all the proteins examined, lyophilization leads to a marked increase in the percentages of β-sheets, with a parallel drop in the percentages of α-helices and unordered structures.

MATERIALS AND METHODS

Materials. Bovine pancreatic trypsin inhibitor (BPTI), RNase A (90 Kunitz units/mg of protein), chymotrypsinogen A, porcine insulin (Zn^{2+} content of 0.5%), horse myoglobin (Mb) (95–100% purity), and cytochrome *c* (Cyt *c*) from the heart of tuna (98% purity), rabbit (97% purity), pigeon (99% purity), chicken (100% purity), horse (99% purity), dog (99% purity), and cow (99% purity) were obtained from Sigma. Recombinant human albumin (rHA) was a generous gift from Delta Biotechnology (Nottingham, U.K.). KBr for making pellets was from SpectraTech (Stamford, CT); acetone, propanol and D-sorbitol were from Aldrich.

Lyophilization. All aqueous protein solutions to be lyophilized were frozen in liquid nitrogen and applied to a Labconco (Kansas City) model 8 freeze-drier at a pressure of approximately 10 μm of Hg and a condenser temperature of −50°C for at least 24 h. Concentrations of all proteins, except for BPTI, were 10 mg/ml in distilled water unless stated otherwise. BPTI and D-sorbitol were lyophilized, separately or together, from a concentration of 1 mg/ml at pH 3.5. The pH of solutions from

Abbreviations: BPTI, bovine pancreatic trypsin inhibitor; Cyt *c*, cytochrome *c*; FTIR, Fourier-transform infrared; rHA, recombinant human albumin; Mb, myoglobin.

*To whom reprint requests should be addressed.

which proteins were lyophilized (adjusted by adding 0.1 N NaOH or HCl) was chosen to allow comparison with spectroscopic results in the literature. For BPTI, it was pH 3.5 for comparison with results of Desai *et al.* (13). Mb was lyophilized from pH 7.0 since the crystals used for x-ray crystallography (28) were grown at this pH (29). For the same reason, pH 4.5 was chosen for chymotrypsinogen (30), pH 5.7 was chosen for RNase A (31), and pH 6.4 was chosen for horse heart Cyt *c* (32). All other cytochromes were studied at pH 6.4 to allow comparison with the horse heart protein. rHA was lyophilized from pH 7.3 (33); the x-ray data were obtained at neutral pH (34). Insulin was lyophilized from pH 4.0.

Alternative Drying Methods for BPTI. Rotary evaporation and acetone precipitation were performed as described (35). Precipitation of BPTI from aqueous solution (100 mg/ml; pH 3.5) with propanol was the same as with acetone.

FTIR Measurements. FTIR spectra were measured by using a Nicolet Magna-IR System 550 optical bench equipped with a MCT-B liquid-N_2-cooled detector (11,700–400 cm^{-1}), Ge beam splitter on KBr substrate (7400–350 cm^{-1}), and a high-intensity, air-cooled mid-IR Ever-Glo source (9600–50 cm^{-1}). The system, with a resolution specification of 0.5 cm^{-1}, was controlled via an interface card by an analytical workstation (486DX266 Intel processor). The system was aligned by using the Nicolet OMNIC 1.2 software before the measurements and every 3 h thereafter. The data collection and calculation of second derivative spectra were carried out with the same software. The optical bench was purged with dry N_2 to reduce interfering water vapor IR absorption.

The solution spectra of proteins in H_2O were measured using a 15-μm spacer (36) in a SpectraTech liquid cell equipped with CaF_2 windows. Aqueous solutions of the original proteins and of the reconstituted powders were measured at the same pH and concentration (2.5–5%). Protein powders were measured at 1 mg of protein per 200 mg of KBr. After homogenizing the lyophilized protein and KBr with an agate mortar and pestle, the powders were pressed into pellets by using a SpectraTech Macro-Micro KBr Die Kit and a Carver Laboratory (Menomonee Falls, WI) 12-ton hydraulic press. This method introduces no artifactual structural changes (14, 15). We verified that no appreciable water was absorbed during the procedure by measuring KBr pellets without protein. A total of 256 scans at 2 cm^{-1} resolution using Happ–Genzel apodization were averaged (14, 15).

When necessary, spectra were corrected for the background in an interactive manner. Subtraction of the water background for aqueous solutions was accomplished by using the Nicolet OMNIC 1.2 software with the following goals: (*i*) a straight baseline in the region of 1800–2500 cm^{-1}, where proteins do not absorb (20), and (*ii*) disappearance of the broad band around 800 cm^{-1} (19). For BPTI precipitated with acetone and co-lyophilized with D-sorbitol, the subtraction was performed on dry samples. In the former case, the spectrum revealed residual acetone even after vacuum drying at 10 μm of Hg for 24 h. The typical acetone IR absorption bands were subtracted to obtain the undisturbed protein vibrational spectrum. Correction for D-sorbitol was performed on the basis of the disappearance of the D-sorbitol IR bands in the fingerprint region (37) of the spectrum. D-Sorbitol was lyophilized under conditions identical to those in its 1:1 (wt/wt) mixture with BPTI. This mixture was measured at 2.4 mg of BPTI per 200 mg of KBr and at 1.2 mg of D-sorbitol per 200 mg of KBr; the latter was used for subtraction.

Each protein sample was measured at least five times. Each spectrum was corrected for the background to obtain the protein vibrational spectra and then analyzed by second derivatization (38, 39) and Gaussian curve fitting (21, 40). The determined peak wavenumbers of the second derivative spectra, as well as those and areas of the fitted Gaussian bands, were averaged, and the standard deviations were calculated. All spectra were analyzed by second derivatization in the amide I and III band regions for their component composition by using the OMNIC 1.2 software. Second derivative spectra were smoothed with an 11-point smoothing function (10.6 cm^{-1}) by using this software.

Overall structural changes occurring upon protein dehydration were quantified by calculating the correlation coefficient *r* (14, 15) from the second derivative spectra in the amide I and III spectral regions. The *r* value reflects differences of two spectra: for identical ones it is 1, for those with nothing in common it is 0. The second derivative spectra used were stored as ASCII *xy* pair data sets (one set of data per cm^{-1}), and the correlation coefficients were calculated by using the SIGMA PLOT program for each individual spectrum of each sample with respect to the averaged reference spectrum.

Gaussian curve fitting was performed by using the GRAMS/386 program (Galactic Industries, Salem, NH) on the original (nonsmoothed) protein vibrational spectra. The number of components and their peak positions were determined by second derivatization (38, 39) and used as starting parameters. After optimization (40), each fit was performed without fixing the peak wavenumber, full width at half maximum, or height of individual bands. Note that due to a better separation of the individual bands, the problems encountered in the analysis of the amide I region, leading to some subjectivity (18, 40), are abolished. In all cases, a linear baseline was fitted (20, 21). The secondary structural element content was calculated from the areas of the individual assigned bands and their fraction of the total area in the amide III region.

Band Assignment in the Amide III Region. Table 1 summarizes the results of the component analysis by second derivatization and the secondary structure quantification by Gaussian curve fitting in the amide III region for the proteins studied. In most cases, the discrepancy between the peak maxima determined by these two methods was below 3 cm^{-1}. Larger deviations observed for some components are still in the range of published ones (21). The assignment of individual components to secondary structural elements was as follows: α-helix, 1293–1328 cm^{-1}; β-sheet, 1225–1250 cm^{-1}, and others, 1257–1288 cm^{-1} (21). We independently verified every assignment by comparison with x-ray structures, as well as with secondary-structure estimates from FTIR spectra in the amide I region (17) and circular dichroism estimates (41, 42) when available.

For proteins containing significant fractions of both α-helix and β-sheet elements (BPTI, chymotrypsinogen, RNase A), the agreement between the secondary structure contents in Table 1 and the literature x-ray data is excellent. For BPTI in solution at pH 9.0, the calculated α-helix and β-sheet contents of 19% ± 2% and 40% ± 1%, respectively, were very similar to those at pH 3.5 and 7.0 (Table 2) and agree with values of 26% α-helix and 45% β-sheet derived from the x-ray studies (43–45). The FTIR-derived parameters for RNase A (23% ± 2% α-helix and 45% ± 2% β-sheet) agree with those calculated (45) from the x-ray data (23% α-helix and 45% β-sheet), as well as with other FTIR (21% α-helix and 50% β-sheet) (17) and circular dichroism data (26% α-helix and 44% β-sheet) (41). Finally, our data for chymotrypsinogen (13% α-helix and 41% β-sheet) agree with those from x-ray (11% α-helix and 46% β-sheet) (45, 46), other FTIR (21% α-helix and 50% β-sheet) (17) and circular dichroism (9% α-helix and 36% β-sheet) (42) studies.

An assignment issue has to be addressed concerning proteins with high α-helix contents (Mb, Cyt *c*, and rHA). FTIR studies in the amide I region have demonstrated that the extended chains connecting the α-helix cylinders absorb at frequencies similar to those of β-sheets (17). This is also the case in the amide III region at 1245 cm^{-1} (26). We indeed observed a band at 1246 cm^{-1} for these proteins and no

Table 1. Infrared band positions in the amide III spectral region of various proteins, band areas determined by the Gaussian curve fitting, and band assignments

Protein	Band position*		Area, %*	Assignment†
	Second derivative	Curve fitting		
BPTI				
Solution	1317 ± 1	1316 ± 1	8 ± 1	α-Helix
	1306 ± 2	1304 ± 1	1 ± 1	α-Helix
	1290 ± 1	1292 ± 1	12 ± 3	α-Helix
	1282 ± 1	1277 ± 3	25 ± 6	Unordered
	1263 ± 0	1262 ± 1	18 ± 9	Unordered
	1247 ± 1	1249 ± 1	6 ± 2	β-Sheet
	1237 ± 1	1238 ± 0	30 ± 1	β-Sheet
Powder	1315 ± 1	1312 ± 2	5 ± 2	α-Helix
	1304 ± 2	‡	‡	α-Helix
	1288 ± 0	1284 ± 1	12 ± 2	Unordered
	1263 ± 1	1262 ± 1	28 ± 2	Unordered
	1246 ± 2	1246 ± 1	10 ± 2	β-Sheet
	1234 ± 1	1233 ± 1	45 ± 2	β-Sheet
RNase A				
Solution	1318 ± 0	1321 ± 0	4 ± 0	α-Helix
	1310 ± 2	1311 ± 0	9 ± 0	α-Helix
	1293 ± 0	1296 ± 1	10 ± 2	α-Helix
	1283 ± 1	1281 ± 3	8 ± 2	Unordered
	1264 ± 1	1261 ± 1	23 ± 3	Unordered
	1249 ± 0	1251 ± 1	4 ± 1	β-Sheet
	1236 ± 1	1238 ± 0	42 ± 2	β-Sheet
Powder	1313 ± 0	1311 ± 0	12 ± 0	α-Helix
	1293 ± 1	1290 ± 1	6 ± 1	α-Helix
	1283 ± 1	1276 ± 2	7 ± 0	Unordered
	1262 ± 0	1263 ± 1	9 ± 0	Unordered
	1245 ± 1	1253 ± 2	4 ± 3	β-Sheet
	1233 ± 0	1236 ± 2	62 ± 3	β-Sheet
Chymotrypsinogen				
Solution	1318 ± 0	1318 ± 0	3 ± 0	α-Helix
	1303 ± 0	1303 ± 1	10 ± 1	α-Helix
	1288 ± 1	1284 ± 0	15 ± 1	Unordered
	1280 ± 1	1277 ± 0	3 ± 1	Unordered
	1266 ± 1	1265 ± 0	13 ± 1	Unordered
	1256 ± 1	1257 ± 2	15 ± 1	Unordered
	1248 ± 0	1246 ± 0	15 ± 1	β-Sheet
	1234 ± 0	1236 ± 1	11 ± 1	β-Sheet
	§	1228 ± 1	15 ± 2	β-Sheet
Powder	1312 ± 0	1308 ± 1	8 ± 0	α-Helix
	1283 ± 1	1282 ± 0	11 ± 0	Unordered
	1262 ± 1	1260 ± 0	23 ± 0	Unordered
	1247 ± 1	1247 ± 1	3 ± 1	β-Sheet
	1232 ± 1	1233 ± 0	55 ± 0	β-Sheet
rHA				
Solution	1320 ± 0	1316 ± 1	30 ± 1	α-Helix
	1303 ± 0	1302 ± 1	1 ± 0	α-Helix
	1293 ± 0	1295 ± 1	27 ± 4	α-Helix
	1281 ± 1	1276 ± 1	15 ± 3	Unordered
	1266 ± 2	1264 ± 0	4 ± 1	Unordered
	1244 ± 1	1246 ± 1	23 ± 1	Extended chain
	1227 ± 1	1226 ± 2	<1%	β-Sheet
Powder	1312 ± 0	1310 ± 0	23 ± 1	α-Helix
	1302 ± 1	1294 ± 1	7 ± 0	α-Helix
	1287 ± 1	1282 ± 1	10 ± 1	Unordered
	1277 ± 1	1274 ± 1	4 ± 1	Unordered
	1262 ± 1	1263 ± 0	11 ± 1	Unordered
	1240 ± 1	1247 ± 1	29 ± 1	Extended chain
	1221 ± 0	1227 ± 0	16 ± 1	β-Sheet
Horse heart Cyt c¶				
Solution	§	1325 ± 2	1 ± 1	α-Helix
	1315 ± 0	1315 ± 1	22 ± 2	α-Helix
	1300 ± 1	1298 ± 1	13 ± 2	α-Helix
	1283 ± 2	1282 ± 0	14 ± 2	Unordered
	1276 ± 1	1274 ± 1	1 ± 1	Unordered
	1264 ± 1	1267 ± 1	19 ± 1	Unordered
	1244 ± 0	1243 ± 2	27 ± 3	Extended chain
	1235 ± 0	1233 ± 1	3 ± 2	β-Sheet
Powder	§	1325 ± 2	5 ± 2	α-Helix
	1312 ± 1	1310 ± 0	12 ± 4	α-Helix
	1303 ± 1	1298 ± 2	6 ± 1	α-Helix
	1284 ± 0	1284 ± 1	14 ± 3	Unordered
	≈1270	1272 ± 2	4 ± 2	Unordered
	1263 ± 0	1261 ± 2	20 ± 4	Unordered
	1244 ± 1	1249 ± 1	3 ± 2	Extended chain
	1237 ± 0	1239 ± 1	23 ± 5	β-Sheet
	≈1225	1225 ± 2	12 ± 2	β-Sheet
Mb				
Solution	1319 ± 2	1322 ± 1	10 ± 3	α-Helix
	1314 ± 1	1308 ± 2	34 ± 3	α-Helix
	1296 ± 1	1294 ± 1	9 ± 2	α-Helix
	1279 ± 1	1282 ± 1	10 ± 4	Unordered
	1270 ± 1	1270 ± 2	20 ± 4	Unordered
	1247 ± 0	1247 ± 1	15 ± 2	Extended chain
	1233 ± 2	1230 ± 2	1 ± 1	β-Sheet
	1221 ± 0	1222 ± 1	1 ± 1	β-Sheet
Powder	1311 ± 0	1312 ± 1	21 ± 0	α-Helix
	1301 ± 1	1298 ± 0	7 ± 1	α-Helix
	1284 ± 1	1282 ± 1	28 ± 1	Unordered
	1261 ± 0	1259 ± 0	17 ± 1	Unordered
	1245 ± 1	1247 ± 1	2 ± 1	Extended chain
	1233 ± 2	1236 ± 1	19 ± 0	β-Sheet
	1221 ± 1	1218 ± 1	6 ± 1	β-Sheet
Zn-insulin				
Solution	1334 ± 2	1332 ± 2	7 ± 2	α-Helix
	1322 ± 1	1322 ± 2	3 ± 3	α-Helix
	1313 ± 1	1313 ± 1	8 ± 4	α-Helix
	1301 ± 1	1299 ± 2	13 ± 2	α-Helix
	1287 ± 1	1285 ± 2	15 ± 3	Unordered
	1275 ± 1	1275 ± 0	3 ± 3	Unordered
	1265 ± 1	1265 ± 0	18 ± 5	Unordered
	1248 ± 0	1249 ± 1	17 ± 2	β-Sheet
	1235 ± 1	1237 ± 1	15 ± 3	β-Sheet
Powder	≈1330	1327 ± 2	4 ± 2	α-Helix
	1313 ± 0	1312 ± 1	8 ± 1	α-Helix
	1299 ± 1	1294 ± 1	11 ± 1	α-Helix
	1287 ± 0	1281 ± 1	9 ± 0	Unordered
	§	1274 ± 1	3 ± 1	Unordered
	1263 ± 1	1265 ± 1	13 ± 3	Unordered
	1241 ± 1	1251 ± 2	25 ± 7	β-Sheet
	1230 ± 0	1232 ± 4	27 ± 2	β-Sheet

*The ± values are the standard deviations calculated by analyzing three to five individual spectra in each case.

†Unordered structures include turns and random coils. For α-helical proteins, the extended chain secondary structure is given individually to allow comparison with FTIR results obtained in the amide I spectral region (17).

‡This component, visible as a shoulder in the second derivative spectra (see Fig. 1*D*), was not amenable to the Gaussian curve fitting (see Fig. 2*B*) because of its weakness in the original spectra.

§These components were not visible in the second derivative spectra. Nevertheless, the Gaussian curve fitting without them resulted in systematic discrepancies between the original spectra and the sums of the fitted bands. The components therefore had to be used.

¶Very similar parameters were obtained for tuna heart Cyt *c* (data not shown).

Table 2. Correlation coefficients and secondary structure contents for BPTI under different conditions

Protein sample	Correlation coefficient*	Secondary structure, %		
		α-Helix	β-Sheet	Unordered†
Aqueous solution‡				
pH 3.5	1.0	21 ± 2	36 ± 2	43 ± 3
pH 7.0	1.0	20 ± 2	43 ± 1	37 ± 3
pH 9.0	0.99	19 ± 2	40 ± 1	41 ± 3
Powder§				
Lyophilization	0.70	5 ± 2	55 ± 0	40 ± 2
Co-lyophilization with sorbitol	¶	13 ± 2	41 ± 2	46 ± 1
Precipitation with acetone	¶	2 ± 1	63 ± 4	35 ± 4
Precipitation with propanol	0.51	4 ± 1	59 ± 1	37 ± 1
Rotary evaporation	0.46	1 ± 1	72 ± 2	27 ± 1
Redissolved powder‖				
Lyophilization	0.99	20 ± 4	42 ± 2	38 ± 4
Co-lyophilization with sorbitol	0.97	23 ± 2	42 ± 1	35 ± 3
Precipitation with acetone	0.96	21 ± 3	40 ± 2	39 ± 4
Precipitation with propanol	0.98	20 ± 3	40 ± 2	40 ± 4
Rotary evaporation	0.99	25 ± 1	40 ± 2	35 ± 4

*All standard deviations for the correlation coefficients are below 2%. All correlation coefficients are calculated (14, 15) for the amide III region vs. the aqueous solution at pH 3.5.
†Unordered structures include turns and random coil secondary structural elements.
‡Solutions of BPTI in water.
§All powders were obtained from aqueous solution at pH 3.5.
¶The correlation coefficients of these samples could not be calculated. However, residual acetone and sorbitol in the pellets could be subtracted sufficiently to allow for the Gaussian curve fitting.
‖For reconstitution, all dehydrated powders were redissolved in water and measured at pH 3.5 at the same concentration as the reference solutions.

significant bands at 1225–1240 cm^{-1} (Table 1) typical for proteins containing β-sheets (21). Since circular dichroism studies indicate very low β-sheet contents for Cyt *c* and Mb (41), the 1246 cm^{-1} band in these proteins was assigned to the extended chain secondary structures and bands at 1225–1240 cm^{-1} to β-sheet structural elements. For horse heart Cyt *c*, the calculated α-helix content (36% ± 1%) agrees with those derived from both x-ray data (36%) (32) and recent FTIR work using Gaussian curve fitting of the amide I band (36%) (47). Our calculated β-sheet content for this Cyt *c* (3%; Table 3) also agrees with the x-ray (32) and circular dichroism data (41). The secondary structure compositions of oxidized horse and tuna heart Cyt *c* elucidated by our FTIR analysis coincide with those from the x-ray analysis (32, 48). For Mb, our calculated α-helix content (53% ± 2%) is significantly below that estimated from the x-ray structure (80%) (28), although our calculated β-sheet content (2%) agrees with the x-ray and circular dichroism data (41). The secondary structure calculated for rHA (58% ± 4% α-helix; 23% ± 1% extended chain) resembled x-ray estimates (67% α-helix; 33% turns and extended chain) (34).

Table 3. Secondary structure contents of various proteins

Protein*	State†	Secondary structure, %		
		α-Helix	β-Sheet	Unordered‡
BPTI	Solution	21 ± 2	36 ± 2	43 ± 3
	Powder	5 ± 2	55 ± 0	40 ± 2
rHA	Solution	58 ± 4	0	42 ± 3
	Powder	30 ± 1	16 ± 1	54 ± 2
Mb	Solution	53 ± 2	2 ± 1	45 ± 2
	Powder	28 ± 1	25 ± 1	47 ± 2
Horse heart Cyt *c*	Solution	36 ± 1	3 ± 2	61 ± 5
	Powder	23 ± 3	35 ± 2	42 ± 3
Tuna heart Cyt *c*	Solution	34 ± 2	2 ± 1	64 ± 2
	Powder	19 ± 2	34 ± 3	47 ± 2
RNase A	Solution	23 ± 2	45 ± 2	32 ± 2
	Powder	18 ± 1	66 ± 1	16 ± 1
Chymotrypsinogen	Solution	13 ± 1	41 ± 1	46 ± 1
	Powder	8 ± 0	58 ± 1	34 ± 0
Zn-insulin	Solution	30 ± 3	32 ± 4	38 ± 2
	Powder	23 ± 1	52 ± 5	25 ± 4

The secondary structures of proteins, both as an aqueous solution and as lyophilized powder, were calculated from Gaussian curve fitting in the amide III band region.
*For a discussion of the secondary structures calculated in this work compared with those from x-ray studies and other spectroscopic techniques, see *Materials and Methods*.
†The pH values of the protein aqueous solutions were as follows: 3.5 for BPTI, 7.3 for rHA, 7.0 for Mb, 6.4 for both horse and tuna Cyt *c*, 5.7 for RNase A, 4.5 for chymotrypsinogen, and 4.0 for Zn-insulin. The protein powders were obtained by lyophilizing these aqueous solutions.
‡Unordered structures include turns, random coil, and extended chain secondary structural elements.

Our characterization of insulin yielded significantly lower α-helix and higher β-sheet contents (30% and 32%, respectively) than the x-ray structure (53% α-helix and 13% β-sheet) (45, 49). This may be due to differences in the pH used in our study and that for which the x-ray structure was determined (pH 6.6).

The same assignments used for the solutions were employed for the corresponding protein powders. Most spectra of dehydrated proteins were simpler than those in aqueous solutions due to band broadening and disappearance of small bands (Table 1). Upon dehydration, some FTIR bands in the amide III region undergo small shifts, as also observed for the amide I region (14, 15). Despite the observed band broadening in dehydrated protein powders, the separation of individual bands is still sufficient for proper Gaussian curve fitting by using the original vibrational spectra without resolution enhancement [required for the amide I quantification (18)].

RESULTS AND DISCUSSION

Our recent hydrogen isotope-exchange/high-resolution NMR work (13) has unequivocally established that BPTI undergoes significant reversible structural changes upon dehydration. However, the nature of these changes could not be quantified. Consequently, herein we employed an independent methodology, FTIR spectroscopy, to address this issue in the same system. FTIR spectroscopy is one of very few methods that allow for the quantification of protein secondary structural elements in both the amorphous and solution states.

Initially, to confirm the perturbations in BPTI structure upon lyophilization, we compared the IR spectrum of the solid protein with that in aqueous solution by using the second derivative spectra in the amide I and III regions (Fig. 1). This was accomplished by calculating the correlation coefficient r (14, 15) for the spectrum of lyophilized BPTI by using that in solution as a reference (see *Materials and Methods* for details). The calculated values of $r = 0.70$ for the amide III region (Table 2) and $r = 0.73$ for the amide I region were very similar, thereby validating the use of the former spectral region.

To appreciate the significance of a difference of some 0.3 in the r values, we measured solution IR spectra of BPTI at two additional pH values, 7.0 and 9.0, and calculated the correlation coefficients vs. the solution at pH 3.5. The correlation coefficients for the amide III and amide I regions, 1.0 and 0.99 (Table 2) and 0.96 and 0.96 for pH 7.0 and 9.0, respectively, are very close to unity, suggesting no appreciable structural changes, despite the 5.5-pH-unit variation. Hence, we conclude that r is not highly sensitive to structural alterations, since changes in the ionization state of ionogenic groups, which cause spectral differences (50) and undoubtedly at least small conformational perturbations, are not reflected in the calculated numbers. Therefore, the r values obtained for lyophilized BPTI, 0.70 in the amide III region, must represent rather drastic changes in the secondary structure. Thus, our analysis

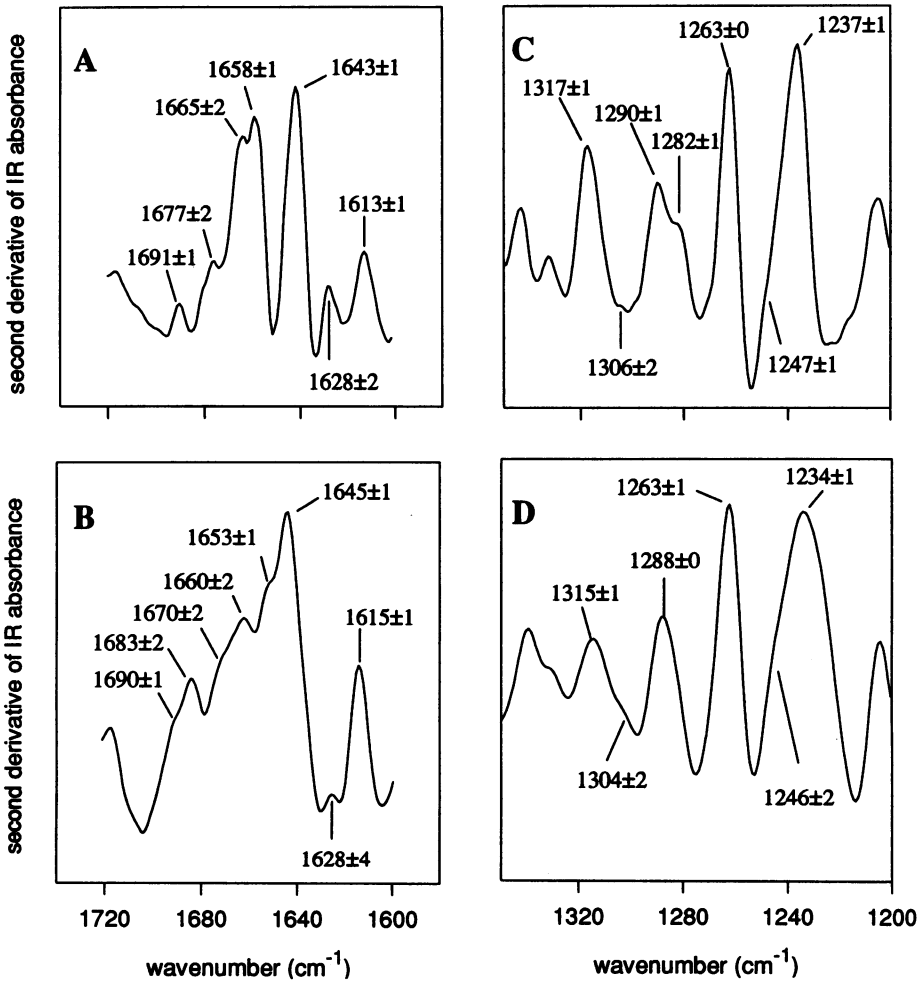

FIG. 1. Second derivative FTIR spectra (multiplied by −1) of BPTI in aqueous solution at pH 3.5 (*A* and *C*) and in the powder obtained by lyophilization from that solution (*B* and *D*). The wavenumbers shown are the average values for the peaks and shoulders from five independent spectra. *A* and *B* depict the amide I region, and *C* and *D* depict the amide III spectral region.

of both spectral regions indicates that BPTI undergoes a significant lyophilization-induced structural rearrangement.

Inspection of the second derivative spectra (Fig. 1) reveals additional structural information not evident from the correlation coefficients. In the BPTI solution spectrum in the amide I region (Fig. 1*A*), two major bands at 1658 and 1643 cm^{-1} are clearly visible. The former with a shoulder at 1665 cm^{-1} can be assigned to α-helix and random coil secondary structural elements, respectively, whereas the latter arises from the β-sheet (16, 51). BPTI lyophilized powder (Fig. 1*B*) has only one major band in this spectral region at 1645 cm^{-1}. The second derivative spectrum of the aqueous solution of BPTI in the amide III region (Fig. 1*C*) shows several well-resolved bands, which were assigned to the secondary structural elements according to Fu *et al.* (21) (Table 1). The major spectral change upon lyophilization (Fig. 1*D*) is a significant broadening (the full width at half maximum increased from 13 ± 1 to 28 ± 2 cm^{-1}) of the band at 1237 cm^{-1} assigned to the β-sheet structural element. Comparison of Fig. 1 *B* and *D* demonstrates the superior band separation in the amide III region in the solid state compared with that in the amide I region.

Inspection of the original spectra in the amide III region qualitatively confirms the pronounced structural changes upon lyophilization (Fig. 2). The spectrum of lyophilized BPTI is dominated by a band at 1238 cm^{-1} (Fig. 2*B*). The bands originating from α-helix and unordered secondary structural elements (1320–1263 cm^{-1}), clearly visible in the solution spectrum (Fig. 2*A*), appear only as shoulders in the lyophilized powder spectrum (Fig. 2*B*). This indicates a conversion from α-helix/unordered structure to β-sheet structural elements.

Comparison of the original and second derivative spectra and the calculation of correlation coefficients, while instructive, yield no quantitative information about variations in the α-helix and β-sheet contents. To quantify the structural changes occurring upon lyophilization of BPTI, we performed Gaussian curve fitting of the IR spectra in the amide III region (Fig. 2). The results (Table 2) reveal a drop in the α-helix content from 21% to 5% and a rise in the β-sheet content from 36% to 55% upon lyophilization. These data provide a quantitative confirmation of the previous qualitative observations (13).

Desai *et al.* (13) further demonstrated that co-lyophilization with the lyoprotectant sorbitol lowered the magnitude of BPTI's structural rearrangement. We found (Table 2) that BPTI co-lyophilized with sorbitol has a secondary structure similar to that observed in solution. In particular, the β-sheet content is essentially the same, indicating that the protein core [which consists mainly of antiparallel β-sheets (43, 44)] is conserved. Note, however, that the content of α-helices in BPTI, located on the periphery of the molecule (43, 44), is not fully conserved. The 13% α-helix content of BPTI in the co-lyophilizate with sorbitol is between that of the lyophilized powder (5%) and that in aqueous solution (21%). The calculated correlation coefficients (for amide I region) also reflect this partial structural preservation: 0.84 for the co-lyophilizate vs. 0.73 for BPTI lyophilized in the absence of sorbitol.

To distinguish whether the observed structural changes in BPTI are caused by the dehydration of the protein *per se* or are specific to lyophilization, we explored alternative drying methods: precipitation with acetone or propanol and rotary evaporation. When compared with the lyophilized powder, the resultant dried samples yielded correlation coefficients (Table 2) indicative of larger structural changes. This is also seen in the secondary structural compositions (Table 2). In particular, in the case of rotary evaporation, there is nearly twice as large an increase in the β-sheet content when compared with lyophilization, and most of this rise comes from the drop in the unordered structure content. These findings are consistent with those obtained by hydrogen isotope exchange/NMR (35), which demonstrated the superiority of lyophilization in conserving BPTI's native structure compared with the alternative dehydration methods.

Having established that BPTI's secondary structure undergoes major rearrangements upon dehydration, an important question was whether this phenomenon is reversible. To answer it, all dehydrated BPTI samples were redissolved in water (pH 3.5), and their IR solution spectra were determined. The *r* values for these solutions vs. the protein solution prior to dehydration, as well as the secondary structure contents, show unequivocally (Table 2) that all dehydration-induced structural changes were fully reversible.

Our BPTI data reveal that the α-helix content decreases and the β-sheet content increases upon dehydration. It was important to establish whether this is a general phenomenon. To this end, we lyophilized 12 different proteins and quantified their secondary structural compositions from the IR spectra.

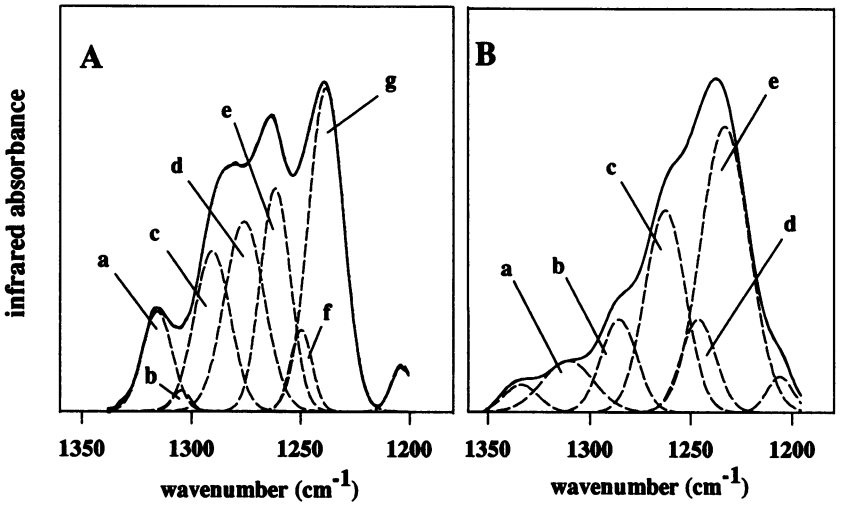

FIG. 2. FTIR spectra of BPTI in aqueous solution at pH 3.5 (*A*) and the powder lyophilized from that solution (*B*) after the Gaussian curve-fitting process. The results of the added Gaussian bands and the original spectra (solid lines) are superimposed and are nearly identical. The area of the individual Gaussian bands (broken lines) has been used to calculate the secondary structure content. The individual bands were assigned as follows: (*A*) a, b, and c, α-helix; d and e, unordered; f and g, β-sheet; (*B*) a, α-helix; b and c, unordered; d and e, β-sheet. The bands at ≈1205 cm^{-1} are not an amide III vibration (21) and are presented solely for the fit. The band at around 1340 cm^{-1} in the spectrum of the powder (*B*), which is of an unknown origin and not found in the BPTI spectrum in aqueous solution, was not assigned to any secondary structural element.

Among the proteins studied, there were seven forms of Cyt *c* (from dog, rabbit, pigeon, chicken, bovine, horse, and tuna hearts). Despite some differences in their primary structures, the IR spectra for the cytochromes were virtually identical both in solution and in the lyophilized states. The correlation coefficients calculated for the Cyt *c* solutions vs. the one for the horse heart Cyt *c* solution (pH 6.4) in the amide III region were all >0.93 with the exception of tuna Cyt *c* ($r = 0.87$). Moreover, the correlation coefficients for the spectra of all lyophilized Cyt *c*s vs. the one for lyophilized horse Cyt *c* were all ≥0.97. Therefore, hereafter we consider only the FTIR data for the two most dissimilar cytochromes, those from horse and tuna hearts.

Table 3 summarizes the secondary structures calculated for eight proteins in solution and in the lyophilized state. [We also quantified the secondary structural elements of the proteins following their reconstitution in water (data not shown) and established that *all* structural changes caused by lyophilization were reversible.] It is seen that all the proteins studied exhibited pronounced secondary structural changes upon lyophilization: in every case, the α-helical content decreased and the β-sheet content increased significantly, although the magnitude of this effect varied among the proteins.

Of the proteins studied, rHA exhibited the largest decrease in α-helical content upon lyophilization, from 58% to 30%. Its β-sheet content rose from 0% to 16%, and the unordered secondary structure rose from 42% to 54%. It is noteworthy that rHA is the only protein in our study to exhibit an increase in unordered structure, indicating that this protein partially unfolds upon lyophilization.

The data for Mb show a precipitous drop in the α-helix content and a parallel increase in the β-sheet content, while the fraction of unordered structures remains the same. For both cytochromes, significant decreases in the α-helical content and ≈10-fold increases in β-sheet content occurred upon dehydration. The unordered structure of both cytochromes decreased substantially, suggesting a higher structural order in the lyophilized state. For RNase A, chymotrypsinogen, and insulin, only minor decreases in the α-helix content but substantial increases in the β-sheet content took place upon lyophilization. For lyophilized insulin, these dehydration-induced structural changes are in line with recent Raman spectroscopy findings comparing bovine Zn-insulin powders with those dissolved in aqueous solutions (52). Note that for all three proteins the percentage of the unordered structures drops upon lyophilization indicating an overall increase in the structural order.

For every protein studied, even those belonging to different structural classes (17), we observed a decrease in α-helices and a concomitant increase in β-sheets upon lyophilization (Fig. 3). Similar behavior was reported for poly(L-lysine) (15), where, regardless of the secondary structure in aqueous solution, the lyophilized polypeptide mainly consisted of β-sheets. It has been predicted that dehydration should induce major structural changes in proteins (53). For instance, Barlow and Poole (54) demonstrated that water molecules hydrogen bond to the C=O groups of the peptide backbone in α-helical but not β-sheet regions; therefore, dehydration should disrupt the former but not the latter portions of the protein molecule. The most likely reason for a marked increase in the β-sheet content of the proteins upon dehydration appears to be formation of intermolecular β-sheet structures, which are entropically prohibitive in solution. In the solid—e.g., lyophilized form—where protein molecules are forced into contact with each other and there is no competing bulk water molecules, such intermolecular interactions presumably become energetically attractive.

The secondary structural transitions depicted in Fig. 3 have also been reported for adsorption of proteins to surfaces. The adsorption of human serum albumin to polymeric contact lens

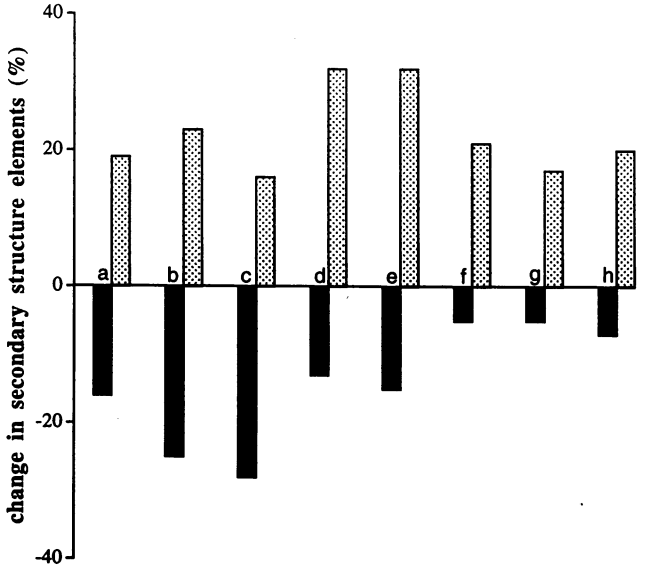

FIG. 3. Changes in the α-helix (solid bars) and β-sheet (dotted bars) content upon lyophilization, as determined by the Gaussian curve fitting of the FTIR spectra of aqueous solutions and lyophilized powders for the following proteins: a, BPTI; b, Mb; c, rHA; d, horse heart Cyt *c*; e, tuna heart Cyt *c*; f, RNase A; g, chymotrypsinogen, and h, insulin.

material is accompanied by a conversion of α-helices and random coils to β-sheets (55). Under these conditions, lysozyme undergoes an α-helix to β-sheet conversion (56) and mucin undergoes a random coil to β-sheet conversion (57). Another example is the adsorption of fibronectin to polyurethane surfaces, which induces a random coil to β-sheet conversion (24).

More closely related to the dehydration-induced structural changes reported herein are those accompanying protein aggregation, another process resulting in increased protein–protein contacts. Thermal aggregation raises the β-sheet content in acetylcholinesterase (58) and ovalbumin (59). Precipitation with salt increases the β-sheet content and decreases the α-helix content of proteins (60). Aggregation of the M13 coat protein (61) and inclusion-body formation of β-lactamase (62) also increase β-sheet content. Finally, an α-helix to β-sheet conversion parallels the solubility decrease in insulinotropin (63).

In summary, by means of FTIR spectroscopy, we found that upon dehydration proteins undergo a marked reversible change in secondary structure: the β-sheet content goes up while the α-helix content goes down. For almost all the proteins studied, lyophilization makes the protein structure more ordered by decreasing the percentage of unordered structures. These structural changes must be considered in analyzing the behavior of dry proteins.

We thank Profs. Robert Langer and Jonathan King and Dr. Henry R. Costantino for helpful discussions. We also thank Dr. Henry R. Costantino for preparing rHA for FTIR measurements. This work was funded by National Institutes of Health Grant GM26698 and the Biotechnology Process Engineering Center at the Massachusetts Institute of Technology.

1. Costantino, H. R., Langer, R. & Klibanov, A. M. (1994) *J. Pharm. Sci.* **83,** 1662–1669.
2. Klibanov, A. M. (1990) *Acc. Chem. Res.* **23,** 114–120.
3. Careri, G., Giansanti, A. & Gratton, E. (1979) *Biopolymers* **18,** 1187–1203.
4. Careri, G., Gratton, E., Yang, P.-H. & Rupley, J. A. (1980) *Nature (London)* **284,** 572–573.
5. Rupley, J. A., Gratton, E. & Careri, G. (1983) *Trends Biochem. Sci.* **8,** 18–22.

6. Rupley, J. A. & Careri, G. (1991) *Adv. Protein Chem.* **41,** 37–172.
7. Schinkel, J. E., Downer, N. W. & Rupley, J. A. (1985) *Biochemistry* **24,** 352–366.
8. Baker, L. J., Hansen, A. M. F., Rao, P. B. & Bryan, W. P. (1983) *Biopolymers* **22,** 1637–1640.
9. Yu, N.-T. & Jo, B. H. (1973) *Arch. Biochem. Biophys.* **156,** 469–474.
10. Poole, P. L. & Finney, J. L. (1983) *Int. J. Biol. Macromol.* **5,** 308–310.
11. Poole, P. L. & Finney, J. L. (1983) *Biopolymers* **22,** 255–260.
12. Gregory, R. B., Gangoda, M., Gilpin, R. K. & Su, W. (1993) *Biopolymers* **33,** 513–519.
13. Desai, U. R., Osterhout, J. J. & Klibanov, A. M. (1994) *J. Am. Chem. Soc.* **116,** 9420–9422.
14. Prestrelski, S. J., Arakawa, T. & Carpenter, J. F. (1993) *Arch. Biochem. Biophys.* **303,** 465–473.
15. Prestrelski, S. J., Tedischi, N., Arakawa, T. & Carpenter, J. F. (1993) *Biophys. J.* **65,** 661–671.
16. Surewicz, W. K. & Mantsch, H. H. (1988) *Biochim. Biophys. Acta* **952,** 115–130.
17. Byler, D. M. & Susi, H. (1986) *Biopolymers* **25,** 469–487.
18. Dòng, A., Prestrelski, S. J., Allison, D. & Carpenter, J. F. (1995) *J. Pharm. Sci.* **84,** 415–424.
19. Singh, B. R., Fuller, M. P. & Schiavo, G. (1990) *Biophys. Chem.* **46,** 155–166.
20. Singh, B. R., DeOliveira, D. B., Fu, F.-N. & Fuller, M. P. (1993) *SPIE* **1890** (Biomol. Spectr. III), 47–55.
21. Fu, F.-N., DeOliveira, D. B., Trumple, W. R., Sakar, H. K. & Singh, B. R. (1994) *Appl. Spectrosc.* **48,** 1432–1441.
22. Kaiden, K., Matsui, T. & Tanaka, S. (1987) *Appl. Spectrosc.* **41,** 180–184.
23. Kato, K., Matsui, T. & Tanaka, S. (1987) *Appl. Spectrosc.* **41,** 861–865.
24. Pitt, W. G., Spiegelberg, S. H. & Cooper, S. L. (1987) in *Proteins at Interfaces*, eds. Brush, J. L. & Horbett, T. A. (Am. Chem. Soc., Washington, DC), pp. 324–338.
25. Wasacz, F. M., Ohlinger, J. M. & Jakobsen, R. J. (1987) *Biochemistry* **26,** 1464–1470.
26. Jakobsen, R. J. & Wasacz, F. M. (1987) in *Proteins at Interfaces*, eds. Brush, J. L. & Horbett, T. A. (Am. Chem. Soc., Washington, DC), pp. 339–361.
27. Singh, B. R., Fu, F.-N. & Ledoux, D. N. (1994) *Struct. Biol.* **1,** 358–360.
28. Evans, S. V. & Brayer, G. D. (1990) *J. Mol. Biol.* **213,** 885–897.
29. Sherwood, C., Mauk, A. G. & Brayer, G. D. (1987) *J. Mol. Biol.* **193,** 227.
30. Wang, D., Bode, W. & Huber, R. (1985) *J. Mol. Biol.* **185,** 595–624.
31. Carlisle, C. H., Palmer, R. A., Mazumdar, S. K., Gorinsky, B. A. & Yeates, D. G. (1974) *J. Mol. Biol.* **85,** 1–18.
32. Bushnell, G. W., Louie, G. V. & Brayer, G. D. (1990) *J. Mol. Biol.* **214,** 585–595.
33. Costantino, H. R., Langer, R. & Klibanov, A. M. (1995) *Bio/Technology* **13,** 493–496.
34. He, X. M. & Carter, D. C. (1992) *Nature (London)* **358,** 209–215.
35. Desai, U. R. & Klibanov, A. M. (1995) *J. Am. Chem. Soc.* **117,** 3940–3945.
36. Singh, B. R. & Fuller, M. P. (1991) *Appl. Spectrosc.* **45,** 1017–1021.
37. Carpenter, J. F. & Crowe, J. H. (1989) *Biochemistry* **28,** 3916–3922.
38. Susi, H. & Byler, D. M. (1983) *Biochem. Biophys. Res. Commun.* **115,** 391–397.
39. Susi, H. & Byler, D. M. (1986) *Methods Enzymol.* **130,** 291–311.
40. Abbott, T. P., Wolf, W. J., Wu, Y. V., Butterfield, R. O. & Kleiman, R. (1991) *Appl. Spectrosc.* **45,** 1665–1673.
41. Provencher, S. W. & Glöckner, J. (1981) *Biochemistry* **20,** 33–37.
42. Chen, Y.-H., Yang, J. T. & Martinez, H. M. (1972) *Biochemistry* **11,** 4120–4131.
43. Huber, R., Kukla, D., Rühlmann, A., Epp, O. & Formanek, H. (1970) *Naturwissenschaften* **57,** 389–392.
44. Deisenhofer, J. & Steigemann, W. (1975) *Acta Crystallogr. B* **31,** 238–250.
45. Levitt, M. & Greer, J. (1977) *J. Mol. Biol.* **114,** 181–293.
46. Freer, S. T., Kraut, J., Robertus, J. D., Wright, H. T. & Xuong, N. H. (1970) *Biochemistry* **9,** 1997–2009.
47. Heimburg, T. & Marsh, D. (1993) *Biophys. J.* **65,** 2408–2417.
48. Takano, T. & Dickerson, R. E. (1981) *J. Mol. Biol.* **153,** 95–115.
49. Blundell, T. L., Dodson, G., Hodkin, D. & Mercola, D. (1972) *Adv. Protein Chem.* **26,** 279–402.
50. Venyaminov, S. Y. & Kalnin, N. N. (1990) *Biopolymers* **30,** 1243–1257.
51. Ohlinger, J. M., Hill, D. M., Jakobsen, R. J. & Brody, R. S. (1986) *Biochim. Biophys. Acta* **869,** 89–98.
52. Yeo, S.-D., DeBenedetti, P. G., Patro, S. Y. & Przybycien, T. M. (1994) *J. Pharm. Sci.* **83,** 1651–1656.
53. Kuntz, I. D., Jr., & Kauzmann, W. (1974) *Adv. Protein Chem.* **28,** 239–345.
54. Barlow, D. J. & Poole, P. L. (1987) *FEBS Lett.* **213,** 423–427.
55. Castillo, E. J., Koenig, J. L., Anderson, J. M. & Lo, J. (1984) *Biomaterials* **5,** 319–325.
56. Castillo, E. J., Koenig, J. L., Anderson, J. M. & Lo, J. (1985) *Biomaterials* **6,** 338–345.
57. Castillo, E. J., Koenig, J. L., Anderson, J. M. & Jentoft, N. (1986) *Biomaterials* **7,** 9–15.
58. Görne-Tschelnokow, U., Naumann, D., Weise, C. & Hucho, F. (1993) *Eur. J. Biochem.* **213,** 1235–1242.
59. Kato, A. & Takagi, T. J. (1988) *Agric. Food Chem.* **36,** 1156–1159.
60. Przybycien, T. M. & Bailey, J. E. (1989) *Biochim. Biophys. Acta* **995,** 231–245.
61. Spruijt, R. B., Wolfs, C. J. A. & Hemminga, M. A. (1989) *Biochemistry* **28,** 9158–9165.
62. Przybycien, T. M., Dun, J. P., Valax, P. & Georgiou, G. (1994) *Protein Eng.* **7,** 131–136.
63. Kim, Y., Rose, C. A., Liu, Y., Ozaki, Y., Datta, G. & Tu, A. T. (1994) *J. Pharm. Sci.* **83,** 1175–1180.